Journal of Materials Chemistry A

PAPER

View Article Online
View Journal | View Issue

Cite this: J. Mater. Chem. A, 2019, 7, 7415

Metal selenide photocatalysts for visible-light-driven *Z*-scheme pure water splitting†

Shanshan Chen, [a] Guijun Ma, [‡b] Qian Wang,[§b] Song Sun,[¶c] Takashi Hisatomi, [a] Tomohiro Higashi, [b] Zheng Wang, [a] Mamiko Nakabayashi,[d] Naoya Shibata,[d] Zhenhua Pan,[b] Toshio Hayashi,[ef] Tsutomu Minegishi, [b] Tsuyoshi Takata[a] and Kazunari Domen [*ab]

Received 21st January 2019
Accepted 28th February 2019

DOI: 10.1039/c9ta00768g

rsc.li/materials-a

Particulate metal selenides having narrow bandgaps for photocatalytic overall pure water splitting have not yet been reported due to the severe self-photooxidation of such materials. The present work demonstrates that solid solutions of zinc selenide and copper gallium selenide (ZnSe:CGSe), with absorption edges ranging from 480 to 750 nm, can be employed as H_2 evolution photocatalysts in particulate photocatalyst sheets for *Z*-scheme pure water splitting, where CoO_x/$BiVO_4$ and Au are used as the oxygen evolution photocatalyst and electron mediator, respectively. Photogenerated holes in the metal selenide are efficiently recombined with electrons from $BiVO_4$ *via* the Au layer, thus avoiding self-oxidation of the selenides and leading to stable pure water splitting. Varying the ZnSe:CGSe composition demonstrates that both the p-type semiconductor character and excellent photoelectrochemical properties of selenides are vital to efficient *Z*-scheme water splitting. This study extends the application field of metal selenides in photocatalytic pure water splitting and creates new opportunities for selenide-based photocatalytic systems for solar fuel production.

Introduction

Sunlight-driven water splitting by particulate photocatalysts has attracted increasing interest as a scalable, low-cost approach to hydrogen production.[1–5] It is a prerequisite to develop highly efficient solar-driven photocatalytic water splitting systems utilizing semiconductors with narrow bandgaps.[6–12] Metal selenide semiconductors have narrower bandgaps than corresponding metal (oxy)sulfides due to shallower valence bands formed by Se 4p orbitals than those formed by O 2p and S 3p orbitals. Besides their narrow bandgap, some other features of stability and flexible band structure together make them extensively investigated in the solar energy conversion field, such as photovoltaic and photoelectrochemical (PEC) cells.[13–15] However, their application in photocatalytic pure water splitting has not been achieved so far, which is mainly because the valence band maxima (VBM) of most selenides are more negative than the water oxidation potential and photogenerated holes preferentially oxidize the selenides themselves (photocorrosion) instead of water. For these reasons, selenide semiconductors have been used only for the hydrogen evolution reaction in the presence of sacrificial reagents.[16] One possible means to apply selenides for overall water splitting is to use them as hydrogen evolution photocatalysts (HEPs) to construct a *Z*-scheme process together with other oxygen evolution photocatalysts (OEPs), but how to efficiently consume photogenerated holes from the selenides before their self-oxidization remains a key issue.[17–20]

Recently, our group has developed a particulate photocatalyst sheet system for *Z*-scheme pure water splitting, in which the HEP and OEP are bridged by a conductive layer that transfers electrons from the OEP to the HEP.[21] Notably, these three components are integrated into one composite having low interfacial resistance, enabling efficient charge transfer and recombination among them. Accordingly, it is considered to

[a]Center for Energy & Environmental Science, Shinshu University, Nagano 380-8553, Japan. E-mail: domen@chemsys.t.u-tokyo.ac.jp
[b]Department of Chemical System Engineering, School of Engineering, The University of Tokyo, Tokyo 113-8656, Japan
[c]National Synchrotron Radiation Laboratory, Collaborative Innovation Center of Chemistry for Energy Materials, University of Science & Technology of China, Hefei 230029, China
[d]Institute of Engineering Innovation, The University of Tokyo, Tokyo 113-8656, Japan
[e]Japan Technological Research Association of Artificial Photosynthetic Chemical Process (ARPChem), Tokyo 113-8656, Japan
[f]Mitsui Chemicals, Inc., Chiba 299-0265, Japan

† Electronic supplementary information (ESI) available: XRD patterns, SEM images, PESA result, Mott–Schottky plots and photocatalytic water splitting. See DOI: 10.1039/c9ta00768g

‡ Current affiliation: School of Physical Science and Technology, Shanghai Tech University, Shanghai 201210, China.
§ Current affiliation: Department of Chemistry, University of Cambridge, Lensfield Road, Cambridge, CB2 1EW, UK.
¶ Current affiliation: School of Chemistry and Chemical Engineering, Anhui University, Hefei 230601, China.

apply the photocorrosive metal selenides in the sheet system to enable pure water splitting.

Herein, we show that particulate photocatalyst sheets for visible-light-responsive *Z*-scheme pure water splitting can be constructed using metal selenides loaded with reduction cocatalysts as HEPs along with $CoO_x/BiVO_4$ and Au as the OEP and electron mediator, respectively. The metal selenides employed here are solid solutions of zinc selenide (ZnSe) and copper gallium selenide (CGSe), which are denoted as ZnSe:CGSe. Copper-containing selenides have been extensively investigated in solar energy conversion systems due to their low toxicity and the possibility of tuning their band structure by using different compositions.[15,22–24] More importantly, by tuning the molar ratio of n-type ZnSe and p-type CGSe, the semiconductor character (p/n type) could also be finely controlled. Therefore, ZnSe:CGSe with different compositions were studied in this work, with the aim of establishing a probable structure-performance relationship. Key factors affecting the *Z*-scheme process and overall water splitting activity were identified, and guidelines for developing selenide-based photocatalytic systems were developed and provided herein.

Experimental

Preparation of photocatalysts

ZnSe:CGSe was prepared by a solid-state reaction based on our previous report.[23] Typically, Cu_2Se (99.9%, High Purity Chemicals), Ga_2Se_3 (99.9%, High Purity Chemicals) and ZnSe (99.99%, High Purity Chemicals) were mixed at Zn/(Zn + Cu) and Ga/Cu molar ratios of 0–1 and 1.0–3.5, respectively, in a glovebox under a nitrogen atmosphere for 30 min. The mixture (1 g in total) was then sealed in a quartz ampule after drying in a vacuum for 2 h. The sealed ampule was then heated at 1173 K for 10 h. After the sample was naturally cooled to room temperature, the product was ground into a powder.

$BiVO_4$ was synthesized *via* a solid–liquid reaction.[25] Typically, 2.40 g of $Bi(NO)_3 \cdot 5H_2O$ (99.99%, Kanto Chemical Co., Inc.) and 0.45 g of V_2O_5 (99.6%, Aldrich) were stirred in 0.75 mol L^{-1} nitric acid aqueous solution (100 mL) for 48 h. The molar ratio of bismuth to vanadium was unity in this suspension. Subsequently, $BiVO_4$ powder was obtained by filtration and washing with distilled water several times before drying. A traditional impregnation and calcination method was used to load a CoO_x cocatalyst on the surface of $BiVO_4$. $Co(NO_3)_2$ (99.5%, Wako Pure Chemical Industries, Ltd.) was used as a cobalt precursor. After impregnating and drying treatments, 0.5 g of the resultant powder was calcined in air at 673 K for 2 h to obtain a $CoO_x/BiVO_4$ photocatalyst. The content of CoO_x (calculated based on the cobalt element) was 0.5 wt% unless otherwise noted.

Preparation of photocatalyst sheets

Photocatalyst sheets based on particulate ZnSe:CGSe and $CoO_x/BiVO_4$ embedded into a Au layer were prepared by the particle transfer method and denoted as ZnSe:CGSe/Au/$BiVO_4$.[21] ZnSe:CGSe and $CoO_x/BiVO_4$ particles (10 mg each) were dispersed in 0.5 mL of isopropanol by sonication for 5 min. The obtained suspension was drop-cast on a glass substrate (3 × 3 cm). After drying naturally at room temperature, a thin Au layer was deposited by vacuum evaporation (VFR-200 M/ERH, ULVAC KIKO, Inc.). Then, a post-annealing treatment at 473 K for 10 min in air was carried out. The resulting Au layer holding the photocatalyst particles was firmly attached to a second glass substrate using adhesive carbon tape (Nisshin EM Co., Ltd.), and then the initial glass plate was lifted off. Excess particles that had piled up on the particle layer were subsequently removed by sonication treatment in distilled water.

Photodeposition of cocatalysts

Nanoparticulate Pt species was photodeposited on the photocatalyst sheet from $H_2PtCl_6 \cdot 6H_2O$ (Kanto Chemicals) in distilled water (40 mL). A Cr_2O_3 layer was subsequently photodeposited from an aqueous K_2CrO_4 (Kanto Chemicals) solution. Here, 0.16 and 0.08 μmol of $H_2PtCl_6 \cdot 6H_2O$ and K_2CrO_4 were used, respectively. The photodeposition reactions were carried out under visible light irradiation ($\lambda > 420$ nm) from a 300 W Xe lamp (CX-04E, INOTEX CO., LTD., Japan) using a closed circulation system for 2 h each.

Photocatalytic pure-water splitting

Z-scheme pure-water splitting reactions were carried out in the same closed gas circulation system with top irradiation using a 300 W Xe lamp equipped with a cut-off filter ($\lambda > 420$ nm). A photocatalyst sheet (3 × 3 cm) was placed at the bottom of the reactor containing 40 mL of distilled water. Before photoirradiation, the reaction system was evacuated to ensure complete air removal. A flow of cooling water was used to keep the reaction suspension at approximately 285 K. Gas chromatography (Shimadzu GC-8A with a thermal conductivity detector, 5 Å molecular sieve columns and Ar carrier gas) was used to analyze the evolved gases.

Quantum yield measurement

The apparent quantum yield (AQY) of *Z*-scheme water splitting was measured using the same experimental setup but with a 420 nm band-pass filter. The number of photons received by the photocatalyst sheet was measured using a grating spectroradiometer (EKO Instruments Co., Ltd., LS-100), and the AQY was calculated using the following equation:

$$\mathrm{AQY}\ (\%) = [4 \times n(H_2)]/n(\mathrm{photons}) \times 100$$

where $n(H_2)$ and n(photons) indicate the number of H_2 molecules generated and the number of incident photons, respectively. It was assumed that all incident photons were absorbed by the photocatalysts. A coefficient of 4 denotes that the two-step photo-excitation processes are involved.

Solar to hydrogen (STH) energy conversion efficiency measurement

The STH value during photocatalytic *Z*-scheme pure-water splitting was measured using the same experimental

apparatus but with illumination from a solar simulator (Asahi Spectra Co., Ltd., HAL-320). The STH value was calculated by the following equation:

$$\mathrm{STH}\ (\%) = [R(\mathrm{H_2}) \times \Delta G]/(P \times S) \times 100$$

where $R(H_2)$, ΔG, P, and S are the rate of hydrogen evolution, the Gibbs free energy for the overall water splitting reaction (H_2O (l) $\rightarrow$ H_2 (g) + $1/2O_2$ (g)), the energy intensity of the solar light irradiation, and the effective irradiation area, respectively. The value of ΔG was 226 kJ mol^{-1} at 285 K at a background pressure of 5 kPa, and the energy intensity of the solar light irradiation was 100 mW cm^{-2}.

Measurement of PEC performance

ZnSe:CGSe and $CoO_x/BiVO_4$ photoelectrodes were prepared by a particle transfer method, which is similar to the preparation process of the ZnSe:CGSe/Au/$BiVO_4$ sheet. A Au layer with a thickness of about 2 μm was deposited by vacuum evaporation on a powder layer, which was drop-cast on a glass substrate. The layers holding the particulate particles were then transferred to another glass plate using adhesive carbon tape. Finally, excess particles piled up on the electrode surface were removed by sonication treatment in distilled water so that only a few particles which were in direct contact with the Au layer remained on the surface. A lead wire was connected to the Au layer of the prepared electrode using indium solder, followed by covering the unnecessary part of the electrode with epoxy resin. A three-electrode setup connected with a potentiostat (HSV-110, Hokuto Denko) was used to deposit a Pt cocatalyst and characterize the PEC properties of the prepared photoelectrodes. A Pt wire and Ag/AgCl electrode were used as the counter and reference electrodes, respectively. For the photo-electrodeposition of a Pt cocatalyst, a solar simulator (XES-401S2, SAN-EI Electric) producing AM 1.5G simulated sunlight at 100 mW cm^{-2} was employed as a light source. A constant potential of −0.8 V *versus* Ag/AgCl was applied to the photoelectrode in an aqueous electrolyte (100 mL) containing 10 μmol L^{-1} H_2PtCl_6, 100 μmol L^{-1} NaOH and 0.1 mol L^{-1} Na_2SO_4 until the saturation of photocurrent. This deposition process lasted for about 1 h. After the Pt deposition, the modified photoelectrode was transferred to another cell containing an aqueous solution (pH 6.9) consisting of 0.1 mol L^{-1} K_2SO_4, 0.025 mol L^{-1} KH_2PO_4, and 0.025 mol L^{-1} Na_2HPO_4 for photoelectrochemical measurements.[26] All of those experiments were performed under purging with an Ar flow.

Materials characterization

The morphologies and elemental compositions of the photocatalyst sheets were assessed by scanning electron microscopy (SEM, S-4700, Hitachi and SU8020, Hitachi) and SEM with energy dispersive X-ray spectroscopy (SEM-EDS, JSM-7001FA, JEOL). X-ray diffraction (XRD) patterns were obtained using a Rigaku MiniFlex 300 powder diffractometer. UV-vis diffuse reflectance spectra (DRS) were recorded with a spectrophotometer (V-670, JASCO) equipped with an integrating sphere, with a Spectralon standard as a reference for baseline correction. To determine the work function of the selenides, photoelectron spectroscopy in air (PESA) was conducted using a surface analyzer (AC-3, Riken-Keiki Co., Ltd). A potentiostat (VersaSTAT 3, Princeton Applied Research) was used for the measurement of Mott–Schottky plots.

Results and discussion

Structural and optical properties of ZnSe:CGSe solid solutions

Fig. 1A and B show the XRD patterns of ZnSe:CGSe samples with a fixed Ga/Cu molar ratio of 2.5 and different Zn/(Zn + Cu) values over the entire compositional range (denoted as $(ZnSe)_x(CuGa_{2.5}Se_{4.25})_{1-x}$). Herein, the samples for which x = 0 and 1 correspond to $CuGa_{2.5}Se_{4.25}$ with a chalcopyrite structure and ZnSe with a zincblende structure, respectively. The $CuGa_{2.5}Se_{4.25}$ specimen was composed of the transition phase of $CuGaSe_2$ and $CuGa_3Se_5$.[23] As shown in Fig. 1B, the diffraction peak at approximately 28° gradually shifted to lower angles with increases in Zn/(Zn + Cu), indicating the formation of solid solutions of $CuGa_{2.5}Se_{4.25}$ and ZnSe. In addition, the peak splitting became smaller as the Zn/(Zn + Cu) value was increased due to the higher symmetry of the $(ZnSe)_x(CuGa_{2.5}Se_{4.25})_{1-x}$ crystal structure.[27] SEM images indicated that the $(ZnSe)_x(CuGa_{2.5}Se_{4.25})_{1-x}$ particles had undefined shapes and that the particle sizes ranged from the submicrometer to micrometer scale (Fig. S1†). Increasing the Zn/(Zn + Cu) ratio produced specimens with larger particle sizes.

To investigate the effect of the Zn/(Zn + Cu) ratio on the band structures of the $(ZnSe)_x(CuGa_{2.5}Se_{4.25})_{1-x}$ semiconductors, UV-vis DRS of those specimens with different Zn/(Zn + Cu) molar ratios were recorded and are given in Fig. 1C. The absorption edge wavelengths of these selenide solid solutions could be tuned over the range of 480–750 nm. With increases in the Zn/(Zn + Cu) value, the absorption edge initially shifted to longer wavelengths and then to shorter wavelengths in a monotonic fashion, and their relationship is depicted in Fig. S2.† The ionization potentials of the materials were determined by PESA to evaluate the relationship between the VBM potential and the Zn/(Zn + Cu) value. Fig. S3† gives the dependence of the photoelectron yield on the incident light energy. It is known that the cube root of photoemission yield ($Y^{1/3}$) is linear to the incident photon energy for semiconductors. The threshold energy corresponds to the ionization potential, which can be determined by the extrapolation method. This obtained energy value is equal to the VBM potential against the vacuum level for semiconductors.[28] It is shown that the threshold energy once decreased as the molar ratio of Zn/(Zn + Cu) increased from 0 to 1/6 and then increased gradually with further increase in the Zn/(Zn + Cu) molar ratio.

The band alignments of the $(ZnSe)_x(CuGa_{2.5}Se_{4.25})_{1-x}$ samples estimated from the band gap energy and VBM potential data are summarized in Fig. 1D. On the basis of thermodynamics, each of these materials would be expected to reduce protons to produce hydrogen and hence is potentially applicable as a HEP. The potentials of the conduction band minimum (CBM) and VBM were dependent on the Zn/(Zn + Cu)

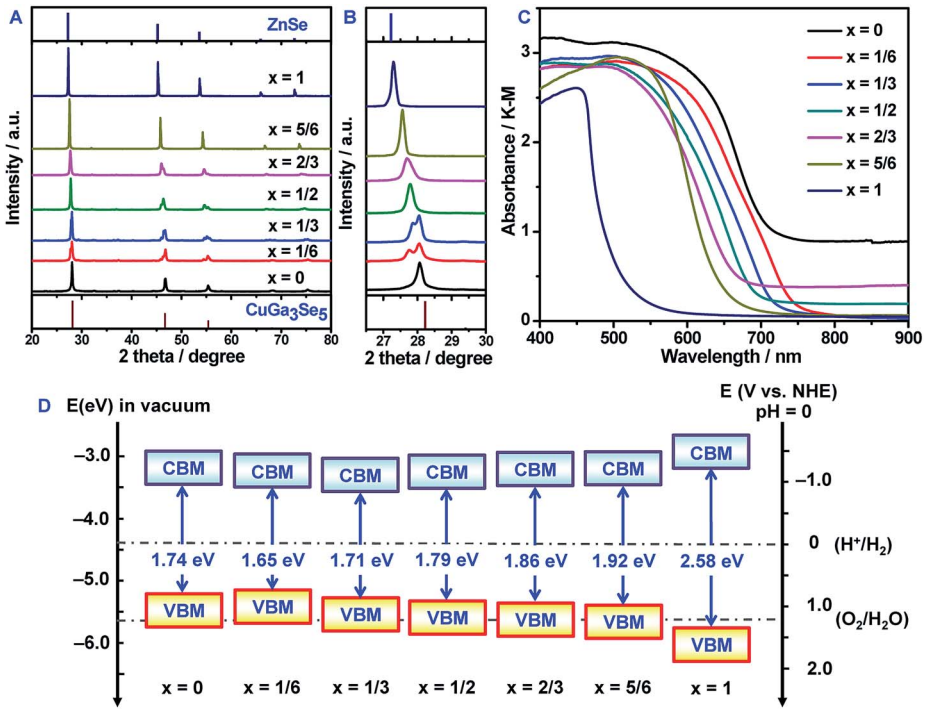

Fig. 1 (A) XRD patterns, (B) enlarged XRD patterns, (C) UV-vis DRS, and (D) estimated band alignments of $(ZnSe)_x(CuGa_{2.5}Se_{4.25})_{1-x}$ solid solutions with various Zn/(Zn + Cu) molar ratios.

molar ratio but not in a monotonic manner. This is exceptional if one considers the change of the constituent elements alone. The CBM and VBM of $(ZnSe)_x(CuGa_{2.5}Se_{4.25})_{1-x}$ are mainly composed of the hybridizations of Zn 4s4p + Ga 4s and Cu 3d + Se 4p orbitals, respectively.[29,30] Judging from the relative band positions of ZnSe and $CuGa_{2.5}Se_{4.25}$, Zn 4s4p forms a conduction band at a higher (more negative) level than Ga 4s, and the introduction of the Cu 3d orbital shifts the VBM potential negatively. This means that the CBM and the VBM of $(ZnSe)_x(CuGa_{2.5}Se_{4.25})_{1-x}$ would be higher and lower than those of $CuGa_{2.5}Se_{4.25}$, respectively. However, the prepared selenides with $x \leq 1/3$ did not follow such a tendency, suggesting contribution from other factors. A similar phenomenon was also reported for the solid solutions of ZnS and $CuGaS_2$, and it was deduced that the distortion of the crystal structure and/or MS_4 tetrahedra and the repulsion between Cu 3d + S 3p and Zn 3d might contribute to the aforementioned anomalous result.[27]

The effects of the Ga/Cu ratio on the structural and optical properties of these ZnSe:CGSe selenides were similarly investigated. Fig. 2A and B show the XRD patterns of $(ZnSe)_{0.5}(CGSe)_{0.5}$ with the Ga/Cu ratios ranging from 1.0 to 3.5. All of the diffraction peaks are assigned to chalcopyrite structures, indicating the formation of solid solutions of ZnSe and CGSe. With increasing the molar ratio of Ga/Cu, the main diffraction peak located at around 28° gradually shifted to higher angles due to rearrangement of the structures.[23] SEM images showed that these materials were composed of particles having undefined morphologies, coarse surfaces and a wide size distribution, ranging from hundreds of nanometers to several micrometers (Fig. S4†). UV-vis DRS (Fig. 2C) and the concluded change of the band gap energy (Fig. S5†) indicated that the band gap energy was increased by approximately 0.1 eV upon increasing the Ga/Cu molar ratio from 1.5 to 3.5. The PESA results demonstrated that the VBM of these selenides was also slightly shifted, from 5.2 to 5.3 eV, upon increasing the Ga/Cu ratio (Fig. S6†). Considering the similarity in these changes, it is thought that the observed increase in the band gap energy can be primarily attributed to the positive shift in the VBM over this composition range. It is known that the repulsion of Cu 3d and Se 4p orbitals can shift the valence band to higher energies in chalcopyrite compounds such as $CuGaSe_2$.[31] Therefore, it can be understood that the positive shift of the VBM is mainly due to the decreased repulsion degree with increases in the Ga/Cu molar ratio.

Photocatalytic performance of ZnSe:CGSe/Au/$BiVO_4$ sheets

Using these ZnSe:CGSe selenides with varying compositions, photocatalyst sheets were fabricated *via* a particle transfer method, together with $CoO_x/BiVO_4$ (see the XRD pattern and UV-vis DRS in Fig. S7†) and Au as the OEP and electron mediator, respectively (Fig. S8†).[21] Top-view SEM and the corresponding EDS mapping images of a representative sheet, where the selenide has a Zn/(Zn + Cu) value of 0.5 and a Ga/Cu ratio of 2.5, are presented in Fig. 3A and S9.† These images demonstrate that both $(ZnSe)_{0.5}(CuGa_{2.5}Se_{4.25})_{0.5}$ and $CoO_x/BiVO_4$ particles cover the Au layer. Cross-sectional SEM images and SEM-EDS mapping images (Fig. 3 and S10†) confirmed that these two different photocatalyst particles were well-distributed and anchored in the Au layer, with a thickness of approximately 500 nm.

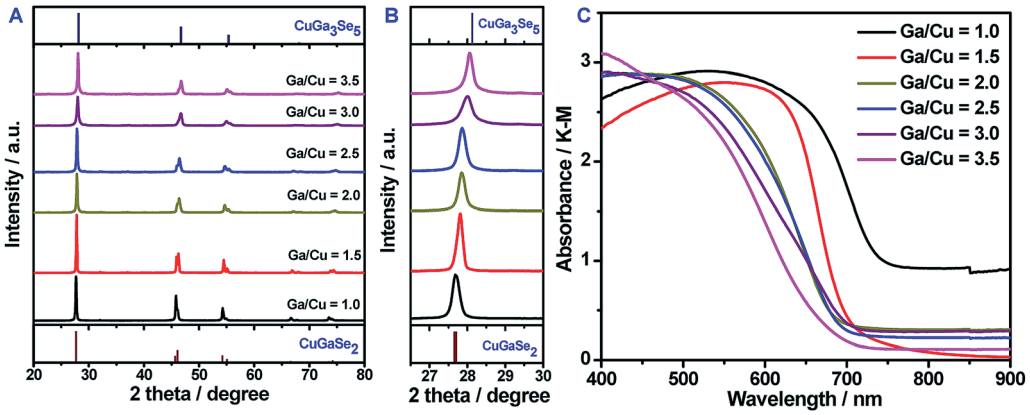

Fig. 2 (A) XRD patterns, (B) enlarged XRD patterns, and (C) UV-vis DRS of a series of $(ZnSe)_{0.5}(CGSe)_{0.5}$ samples with different molar ratios of Ga/Cu.

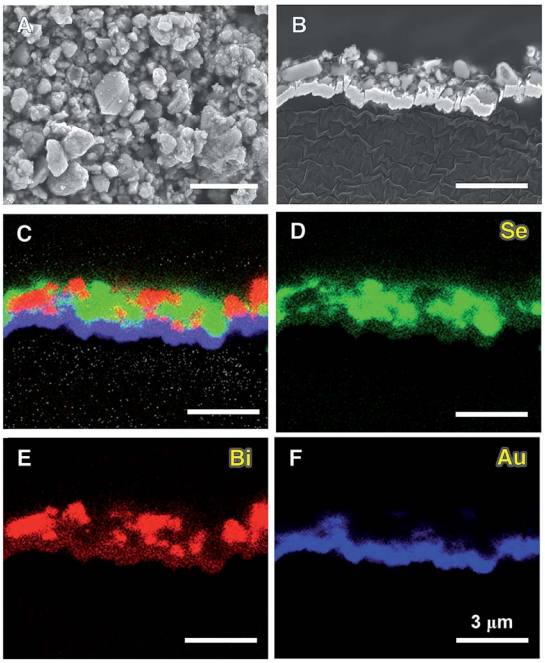

Fig. 3 SEM images and SEM-EDS mapping images of a $(ZnSe)_{0.5}(CuGa_{2.5}Se_{4.25})_{0.5}$/Au/$BiVO_4$ sheet. (A) Top-view and (B) cross-sectional SEM images. SEM-EDS mapping images showing (C) a superimposition of all elements, (D) Se, (E) Bi and (F) Au.

The photocatalytic pure water splitting activities of ZnSe:CGSe/Au/$BiVO_4$ sheets with different values of Zn/(Zn + Cu) and Ga/Cu were evaluated under visible light irradiation. Each sheet was modified with a Pt/Cr_2O_3 cocatalyst prior to the reaction (see the ESI† for details). As shown in Fig. 4A, the incorporation of ZnSe into the $CuGa_{2.5}Se_{4.25}$ significantly affected the photocatalytic activity. The water splitting rate was dependent on the Zn/(Zn + Cu) value in a reversed V-shape, peaking at a ratio of 0.5. When the Zn/(Zn + Cu) value was equal to and greater than 5/6, overall water splitting did not occur. Based on this optimal Zn/(Zn + Cu) ratio, $(ZnSe)_{0.5}(CGSe)_{0.5}$/Au/$BiVO_4$ sheets with different Ga/Cu ratios were subsequently evaluated. As seen from Fig. 4B, there was a similar relationship between the water splitting rate and the Ga/Cu ratio, with the highest activity at a Ga/Cu ratio of 2.5. Time courses of overall water splitting on these sheets indicated that the activity was maintained over the testing time period of 6 h, and the molar ratio of the produced H_2 and O_2 was close to the theoretical value of 2 (Fig. S11 and S12†). The stability test showed that the optimal $(ZnSe)_{0.5}(CuGa_{2.5}Se_{4.25})_{0.5}$/Au/$BiVO_4$ sheet (AQY: 0.54% at 420 nm and STH energy conversion efficiency: 0.01%) could split water in a stable manner over a span of 17 h under visible light irradiation, indicating that the self-oxidation of $(ZnSe)_{0.5}(CuGa_{2.5}Se_{4.25})_{0.5}$ was effectively suppressed (Fig. 4C). For a control sheet sample without the Au layer, only H_2 gas with decreased evolution rate was detected, implying that the *Z*-scheme process was not operational and the selenide photocatalyst underwent photo-corrosion during the reaction (Fig. S13†). That is to say, the successful stable overall water splitting using the selenides in the form of the photocatalyst sheet is primarily due to the conductive Au layer, which facilitates electron transfer from the $BiVO_4$ to the ZnSe:CGSe and allows recombination of the transferred electrons with holes to protect the selenide photocatalysts from being oxidized. This result represents the first-ever demonstration that selenide-based photocatalytic systems can split pure water under visible light irradiation, further extending the application field of metal selenides in solar energy conversion. Considering that absorption edges of selenides are generally longer than those of sulfide and oxide semiconductors composed of the same metal cations, higher solar-to-hydrogen energy conversion efficiency can be theoretically achieved based on selenide semiconductors.[4]

Physical properties of ZnSe:CGSe dominating the performance of the photocatalyst sheets

Our previous work regarding oxysulfide-based sheet systems indicated that overall water splitting activity was strongly correlated with the activity of the HEP as a photocathode rather than as a suspended photocatalyst.[32,33] Therefore, the PEC properties of ZnSe:CGSe semiconductors embedded into a Au

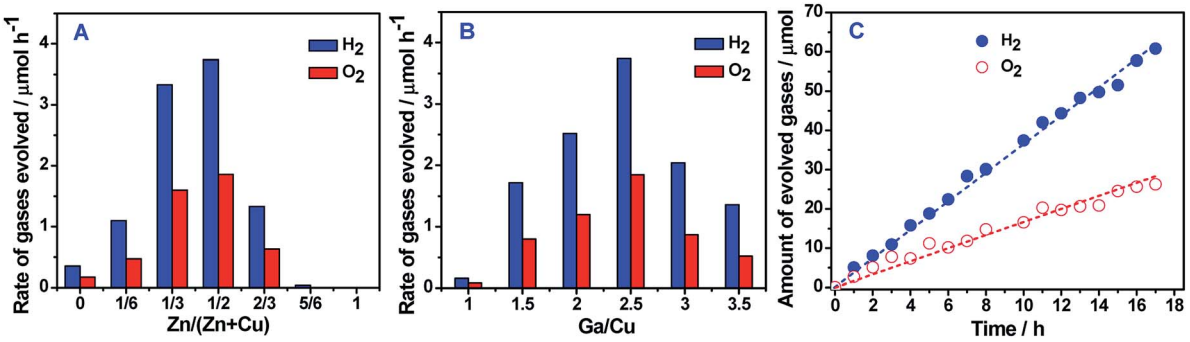

Fig. 4 Gas evolution during photocatalytic overall water splitting using ZnSe:CGSe/Au/$BiVO_4$ sheets under visible light. Photocatalytic overall water splitting activities of (A) $(ZnSe)_x(CuGa_{2.5}Se_{4.25})_{1-x}$/Au/$BiVO_4$ sheets with varying Zn/(Zn + Cu) values and (B) $(ZnSe)_{0.5}(CGSe)_{0.5}$/Au/$BiVO_4$ sheets with varying Ga/Cu ratios. (C) Time courses of the *Z*-scheme water splitting over a $(ZnSe)_{0.5}(CuGa_{2.5}Se_{4.25})_{0.5}$/Au/$BiVO_4$ sheet. Reaction conditions: distilled water (40 mL), light source: 300 W xenon lamp ($\lambda > 420$ nm), irradiation area: 9 cm^2, reduction cocatalyst: 0.16 μmol Pt, Pt/Cr = 2, oxidation cocatalyst: 0.5 wt% CoO_x (with respect to $BiVO_4$).

contact layer and loaded with a Pt cocatalyst were investigated. The Au contact layer and Pt cocatalyst were selected based on the composition of the photocatalyst sheets previously assessed so that their features could be linked with each other. As shown in Fig. 5, these ZnSe:CGSe photoelectrodes generated either cathodic or anodic photocurrents depending on their compositions due to the different semiconductor types. The Mott–Schottky data showed that the $(ZnSe)_x(CuGa_{2.5}Se_{4.25})_{1-x}$ changed from p-type to n-type when the x value reached 5/6 (Fig. S14†). The p/n-type transformation was similarly found for the solid solutions of n-type $CuInSe_2$ and p-type $CuGaSe_2$ with varied compositions.[34] Interestingly, this is also the x value above which the photocatalyst sheets no longer exhibit water splitting activity. Therefore, it is evident that the p-type character of the ZnSe:CGSe semiconductor is a prerequisite to obtaining an effective *Z*-scheme overall water splitting process when assembled with the n-type $BiVO_4$ photocatalyst. This result is similar to the case of *Z*-scheme systems based on reduced graphene oxide as the electron mediator.[26]

It has been reported that *Z*-scheme water splitting systems based on solid-state electron mediators require that the HEP photocathode and OEP photoanode generate photocurrents within the same potential window.[35] As shown in Fig. 5, all p-type selenide photocathodes showed onset potentials more positive than 0.32 V *vs.* RHE, which was the onset potential of the n-type CoO_x/$BiVO_4$ photoanode. In this circumstance, these selenide photocatalysts could be coupled with CoO_x/$BiVO_4$ to obtain a *Z*-scheme process, where electrons from the CoO_x/$BiVO_4$ would be spontaneously transferred *via* the Au layer to the p-type selenide photocatalyst without an external bias. It is also important to note that the trends in the onset potential data are similar to those shown by the photocatalytic activities in Fig. 4A and B. This result confirms that a selenide photocathode having a positive onset potential and a high photocurrent can drive an efficient photocatalytic *Z*-scheme water splitting process. The photocatalyst sheet can be regarded as an assembly of numerous miniature p–n PEC cells.[21] It is required that the used conductive layer should allow the HEP and the OEP to work efficiently in the forms of photocathode and photoanode, respectively. Thus, it is generally favorable to use large

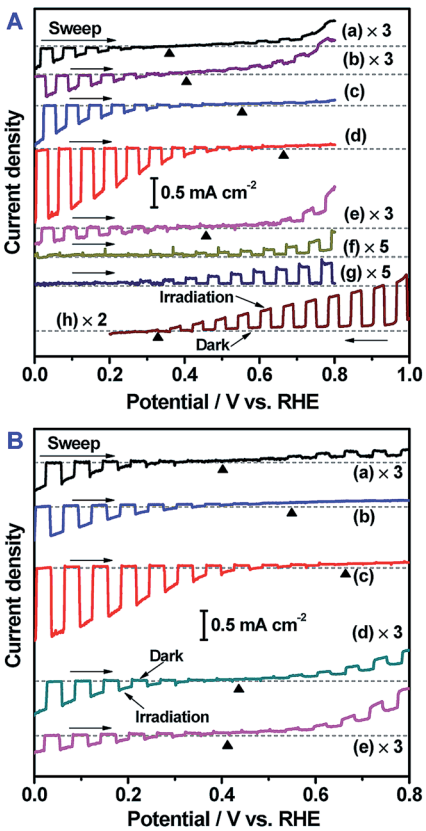

Fig. 5 Current–potential curves of ZnSe:CGSe photoelectrodes with different compositions and a CoO_x/$BiVO_4$ photoelectrode under chopped irradiation. (A) Current–potential curves of $(ZnSe)_x(CuGa_{2.5}Se_{4.25})_{1-x}$ photoelectrodes in which x is (a) 0, (b) 1/6, (c) 1/3, (d) 1/2, (e) 2/3, (f) 5/6 and (g) 1 and (h) a CoO_x/$BiVO_4$ photoelectrode. (B) Current–potential curves of $(ZnSe)_{0.5}(CGSe)_{0.5}$ photoelectrodes with Ga/Cu molar ratios of (a) 1.5, (b) 2.0, (c) 2.5, (d) 3.0, and (e) 3.5. Electrolyte: an aqueous solution (pH 6.9) of 0.1 mol L^{-1} K_2SO_4 + 0.025 mol L^{-1} KH_2PO_4 + 0.025 mol L^{-1} Na_2HPO_4 and light source: AM 1.5G. The dashed lines represent the baselines for the respective electrodes. Based on these baselines, the onset potentials are confirmed at which a sharp increase in photocurrent is detected.

and small work function materials for HEP and OEP materials, respectively, to minimize the Schottky-type barrier. In the present case, Au with a work function as high as 5.1 eV is applicable because the corresponding CoO_x/$BiVO_4$ photoanode can generate decent photocurrent. The photocurrent and working potential of such cells are determined by the intersection of the current–potential curves of the photocathode and photoanode. As such, a photocathode with a more positive onset potential and higher photocurrent will generate higher working photocurrent in a PEC cell. This working photocurrent without an external bias is generally considered as another indicator of photocatalytic activity in a *Z*-scheme water splitting process. The higher the working photocurrent, the easier and more efficient the *Z*-scheme overall water splitting is. Hence, it can be concluded that the PEC characteristics of these materials are closely related to the photocatalytic performance of the particulate photocatalyst sheet system and thus may provide useful information with regard to improving the activity of the system.

Conclusions

This work demonstrated that particulate metal selenides with narrow bandgaps (absorption edges ranging from 480 to 750 nm) could be applied to stable *Z*-scheme pure water splitting. In this photocatalytic system, ZnSe:CGSe photocatalysts were used as HEPs, in conjunction with CoO_x/$BiVO_4$ and Au as the OEP and electron mediator, respectively. The p-type semiconductor character of the ZnSe:CGSe selenides and the presence of a potential window in which the selenide photocathode and $BiVO_4$ photoanode can generate photocurrent are essential to obtaining a *Z*-scheme process. It was also confirmed that the selenides exhibiting a relatively positive onset potential and high photocurrent as photocathodes could achieve higher performance in *Z*-scheme pure water splitting. This study opens up a new application field of photocatalytic pure water splitting for metal selenides and provides insights into the construction of selenide-based *Z*-scheme overall water splitting systems, which are believed to be extended to other solar energy conversion processes.

Conflicts of interest

There are no conflicts to declare.

Acknowledgements

We thank Prof. Akihiko Kudo from the Tokyo University of Science for useful discussions. This work was financially supported by the Artificial Photosynthesis Project of the New Energy and Industrial Technology Development Organization (NEDO) and Grant-in-Aids for Scientific Research (A) (No. 16H02417) and Young Scientist (A) (15H05494) from the Japan Society for the Promotion of Science. Part of this work was conducted at the Advanced Characterization Nanotechnology Platform of the University of Tokyo, supported by the "Nanotechnology Platform" of the Ministry of Education, Culture, Sports, Science and Technology (MEXT), Japan.

Notes and references

1 A. Kudo and Y. Miseki, *Chem. Soc. Rev.*, 2009, **38**, 253–278.
2 D. M. Fabian, S. Hu, N. Singh, F. A. Houle, T. Hisatomi, K. Domen, F. E. Osterloh and S. Ardo, *Energy Environ. Sci.*, 2015, **8**, 2825–2850.
3 M. R. Shaner, H. A. Atwater, N. S. Lewis and E. W. McFarland, *Energy Environ. Sci.*, 2016, **9**, 2354–2371.
4 S. Chen, T. Takata and K. Domen, *Nat. Rev. Mater.*, 2017, **2**, 17050.
5 D. Kong, Y. Zheng, M. Kobielusz, Y. Wang, Z. Bai, W. Macyk, X. Wang and J. Tang, *Mater. Today*, 2018, **21**, 897–924.
6 A. Kudo, *MRS Bull.*, 2011, **36**, 32–38.
7 W. Wang, J. Chen, C. Li and W. Tian, *Nat. Commun.*, 2014, **5**, 4647.
8 P. Zhang, J. Zhang and J. Gong, *Chem. Soc. Rev.*, 2014, **43**, 4395–4422.
9 G. Zhang, G. Liu, L. Wang and J. T. S. Irvine, *Chem. Soc. Rev.*, 2016, **45**, 5951–5984.
10 G. Zhang, Z. Lan and X. Wang, *Chem. Sci.*, 2017, **8**, 5261–5274.
11 Y. Wang, H. Suzuki, J. Xie, O. Tomita, D. J. Martin, M. Higashi, D. Kong, R. Abe and J. Tang, *Chem. Rev.*, 2018, **118**, 5201–5241.
12 L. Wang, Y. Zhang, L. Chen, H. Xu and Y. Xiong, *Adv. Mater.*, 2018, **30**, 1801955.
13 J. F. Guillemoles, L. Kronik, D. Cahen, U. Rau, A. Jasenek and H. W. Schock, *J. Phys. Chem. B*, 2000, **104**, 4849–4862.
14 M. Moriya, T. Minegishi, H. Kumagai, M. Katayama, J. Kubota and K. Domen, *J. Am. Chem. Soc.*, 2013, **135**, 3733–3735.
15 L. Zhang, T. Minegishi, J. Kubota and K. Domen, *Phys. Chem. Chem. Phys.*, 2014, **16**, 6167–6174.
16 F. A. Frame and F. E. Osterloh, *J. Phys. Chem. C*, 2010, **114**, 10628–10633.
17 S. Chen, Y. Qi, C. Li, K. Domen and F. X. Zhang, *Joule*, 2018, **2**, 2260–2288.
18 R. Abe, K. Sayama, K. Domen and H. Arakawa, *Chem. Phys. Lett.*, 2001, **344**, 339–344.
19 P. Zhou, J. Yu and M. Jaroniec, *Adv. Mater.*, 2014, **26**, 4920–4935.
20 H. Li, W. Tu, Y. Zhou and Z. Zou, *Adv. Sci.*, 2016, **3**, 1500389.
21 Q. Wang, T. Hisatomi, Q. Jia, H. Tokudome, M. Zhong, C. Wang, Z. Pan, T. Takata, M. Nakabayashi, N. Shibata, Y. Li, I. D. Sharp, A. Kudo, T. Yamada and K. Domen, *Nat. Mater.*, 2016, **15**, 611–615.
22 C. P. Muzzillo, W. E. Klein, Z. Li, A. D. DeAngelis, K. Horsley, K. Zhu and N. Gaillard, *ACS Appl. Mater. Interfaces*, 2018, **10**, 19573–19579.
23 H. Kumagai, T. Minegishi, Y. Moriya, J. Kubota and K. Domen, *J. Phys. Chem. C*, 2014, **118**, 16386–16392.
24 H. Kaneko, T. Minegishi, M. Nakabayashi, N. Shibata, Y. Kuang, T. Yamada and K. Domen, *Adv. Funct. Mater.*, 2016, **26**, 4570–4577.
25 A. Iwase, Y. H. Ng, Y. Ishiguro, A. Kudo and R. Amal, *J. Am. Chem. Soc.*, 2011, **133**, 11054–11057.

26 K. Iwashina, A. Iwase, Y. H. Ng, R. Amal and A. Kudo, *J. Am. Chem. Soc.*, 2015, **137**, 604–607.
27 T. Kato, Y. Hakari, S. Ikeda, Q. Jia, A. Iwase and A. Kudo, *J. Phys. Chem. Lett.*, 2015, **6**, 1042–1047.
28 J. Kim, T. Minegishi, J. Kubota and K. Domen, *Jpn. J. Appl. Phys.*, 2012, **5**, 015802.
29 C. M. I. Okoye, *Phys. B*, 2003, **337**, 1–9.
30 Y. Zhang, X. Yuan, X. Sun, B. C. Shih, P. Zhang and W. Zhang, *Phys. Rev. B: Condens. Matter Mater. Phys.*, 2011, **84**, 075127.
31 J. E. Jaffe and A. Zunger, *Phys. Rev. B: Condens. Matter Mater. Phys.*, 1983, **27**, 5176.
32 S. Sun, T. Hisatomi, Q. Wang, S. Chen, G. Ma, J. Liu, S. Nandy, T. Minegishi, M. Katayama and K. Domen, *ACS Catal.*, 2018, **8**, 1690–1696.
33 Z. Song, T. Hisatomi, S. Chen, Q. Wang, G. Ma, S. Li, X. Zhu, S. Sun and K. Domen, *ChemSusChem*, 2019, DOI: 10.1002/cssc.201802306.
34 S. Zhang, S. Wei and A. Zunger, *J. Appl. Phys.*, 1998, **83**, 3192.
35 A. Iwase, S. Yoshino, T. Takayama, Y. H. Ng, R. Amal and A. Kudo, *J. Am. Chem. Soc.*, 2016, **138**, 10260–10264.